5-2017

Comparing Multiple Turbulence Restoration Algorithms Performance on Noisy Anisoplanatic Imagery

Michael Armand Rucci
Air Force Research Laboratory

Russell C. Hardie
University of Dayton, rhardie1@udayton.edu

Alexander J. Dapore
L-3 Communications Cincinnati Electronics

Comparing Multiple Turbulence Restoration Algorithms Performance on Noisy Anisoplanatic Imagery

Michael A. Rucci*[a], Russell C. Hardie[b], Alexander J. Dapore[c]
[a]Air Force Research Laboratory, 2241 Avionics Circle, Wright Patterson AFB, OH 45433;
[b]Department of Electrical and Computer Engineering, University of Dayton, 300 College Park, Dayton, Ohio 45459; [c]L3 Technologies Cincinnati Electronics, 7500 Innovation Way, Mason, Ohio 45040

ABSTRACT

In this paper, we compare the performance of multiple turbulence mitigation algorithms to restore imagery degraded by atmospheric turbulence and camera noise. In order to quantify and compare algorithm performance, imaging scenes were simulated by applying noise and varying levels of turbulence. For the simulation, a Monte-Carlo wave optics approach is used to simulate the spatially and temporally varying turbulence in an image sequence. A Poisson-Gaussian noise mixture model is then used to add noise to the observed turbulence image set. These degraded image sets are processed with three separate restoration algorithms: Lucky Look imaging, bispectral speckle imaging, and a block matching method with restoration filter. These algorithms were chosen because they incorporate different approaches and processing techniques. The results quantitatively show how well the algorithms are able to restore the simulated degraded imagery.

Keywords: Imaging, turbulence, anisoplanatism, Monte-Carlo, wave optics, noise, restoration

1. INTRODUCTION

An imaging system is susceptible to a wide range of degradations that limit its performance. In situations where data is captured over long distances, such as in the astronomical case, the limiting factor in the camera's performance is typically due to turbulence.

Turbulence artifacts are due to continual changes in temperature and pressure that lead to random fluctuations in the index of refraction[1]. These continual changes in the atmosphere lead to warping and blurring in collected imagery. The strength of turbulence can be quantified by a C_n^2 profile along the path. Additionally this profile is used to calculate the Fried parameter[1,2] and the isoplanatic angle[1]. Both of these products convey information on how an atmospheric point spread function (PSF) will behave. In cases where the FOV subtends many isoplanatic patches, the turbulent short exposure PSF's now become space variant. This in turn leads to a more challenging case for turbulence mitigation. It is important to note that in either imaging scenario the Fried parameter used for the long exposure case PSF is space invariant.

It is well established there is continual research to simulate and mitigate turbulence. Approaches to simulate turbulence[3,4] allow for truth data to be available to be used in quantifying how well a mitigation approach works on varying levels of turbulence strength. Mitigation methods include, but are not limited to, multi-frame approaches and deblurring[5], Lucky Look[6], or speckle imaging[7,8]. All three methods have different variations in the approach to remove turbulence.

Another consideration in image quality is the signal to noise ratio (SNR). A higher SNR level allows for more contrast in the imagery. However, there are cases where a short integration time is used with the camera to freeze the effects of turbulence. In doing so the signal levels of the imagery remain lower than a long exposure case.

Typically, just as with trying to model and mitigate turbulence, a camera's noise statistics are modeled with an additive Gaussian noise term[9,10]. A more accurate representation of the total camera system noise[11,12] is through a Poisson-Gaussian noise mixture model.

In this paper we combine simulated turbulence with a Poisson-Gaussian noise model to survey how well the three main outlined algorithms perform in restoring the degraded data. Section 2 discusses the modeling/simulation approach. The results of the algorithms are presented in Section 3. Finally, a conclusion is provided in Section 4.

Long-Range Imaging II, edited by Eric J. Kelmelis, Proc. of SPIE Vol. 10204,
1020409 · © 2017 SPIE · CCC code: 0277-786X/17/$18 · doi: 10.1117/12.2269133

2. OBSERVATION MODEL

The forward model used to describe noisy turbulent data stems from previous work[4,13]. In these papers the n^{th} observed image is a culmination of warping and blurring, such that

$$g(x,y)_n = s(x,y)_n\{h(x,y)_{an}[f(x,y)]\} + \eta(x,y)_n. \quad (1)$$

The ideal frame is $f(x,y)$ with x, y being spatial coordinates. A position-dependent shift operator, $s(x,y)_n()$, describes the warping seen in the imagery. In turn, the position-dependent/position corrected blurring is included in $h(x,y)_{an}()$. Note the above model only includes additive iid Gaussian noise, $\eta(x,y)_n$, that has a zero mean with a known variance.

As discussed earlier in and in other papers[11,12], a Poisson-Gaussian noise model is more accurate. Thus, part of the equation above can be rewritten for simplicity as

$$z(x,y)_n = s(x,y)_n\{h(x,y)_{an}[f(x,y)]\}. \quad (2)$$

The warped/blurred image, $z(x,y)_n$, is then added into the Possion-Gaussian noise model to represent the observed frame as

$$g(x,y)_n = \alpha P(\alpha^{-1} z(x,y)_n) + \eta(x,y)_n. \quad (3)$$

In the equation above P is a Poisson random process contributing the signal dependent component of the noise and α is a scalar value representing the camera gain. For the purposes of generic noise modeling, versus a physical cameras performance, we will allow α to be one for the simulations in this paper. In the revised noise mode we have neglected to show a camera offset term as it is typically zero[11].

The camera model used in the turbulence simulations is the same as in a previous paper[4], and shown again for convenience in Table 1.

Table 1. Information on the camera system used in the simulations.

Parameter	Value
Aperture	*D = 0.2034m*
Focal length	*l = 1.2m*
F-number	*f/# =5.9*
Wavelength	*λ = 0.525μm*
Object distance	*L = 7km*
Nyquist pixel spacing (focal plane)	*δ_f = 1.5488μm*
Nyquist pixel spacing (object plane)	*δ_o = 9.0344mm*
Input image dynamic range	*256 digital units*
Additive Gaussian noise variance	*4 digital units*

The camera parameters listed above were chosen to represent a generic imaging system. The wavelength of the system certainly allows for turbulent imagery to be collected over the horizontal slant range of seven kilometers. A input dynamic range of 8 bits was chosen due to the fact the camera would be collecting short exposure imagery to freeze the turbulence. The f-number of the system was also chosen to ensure the system was limited by the turbulent component of the modulation transfer function (MTF).

The turbulence parameters also follow from a previous paper[4] and are given in Table 2. The algorithm used was a Monte-Carlo wave optics approach using a set number of equally spaced phase screens between the object and the camera. Any aspects of camera motion were not incorporated into the simulation data sets generated for this survey. Instead, the camera and object were modeled as remaining stationary during the time of the collection.

Table 2. Information on the turbulence parameters used in the simulations.

Parameter	Value
Path length	*L = 7km*
Propagation step	*Δz = 700m*
Cropped screen samples	*N = 256*
Propagation screen width	*X = 0.9699 m*
Pupil plane point spread	$\widetilde{D}$*= 0.8136 m*
Propagation sample spacing	*Δx = 0.0038m*
Number of phase screens	*N = 10 (9 non-zero)*
Phase screen type	*Modified von Kármán with subharmonics*
Inner scale	l_o*= 0.01m*
Outer scale	L_o*=300m*
Image size (pixels)	*257×257*
Image size (object plane)	*2.3218×2.3218 m*
Pixel skip	*4 pixels (65×65 PSF array)*

These turbulence parameters were used to simulate turbulence over a horizontal path where the C_n^2 would be a constant value.

All turbulent datasets used in this survey were generated by a method discussed in another paper[4] and also used in a restoration paper[5]. The restoration paper however did not use a Poisson-Gaussian noise mixture model. These two papers provide greater details on the specific details used to create the simulated turbulence products. Camera noise was then added after the turbulence was simulated following the equations outlined above.

3. RESULTS

In this section we present a variety of restoration results. Three main algorithms were chosen to process four levels of turbulence. The first algorithm is the block-matching Wiener filter (BMWF) turbulence mitigation system[5]. The main parameters used in the BMWF algorithm is the block matching algorithm (BMA) that had the window size set to 15 ×15 pixels. The other component is the noise to signal ratio (NSR) used in the Wiener filter portion of the algorithm. The algorithm was able to choose the best NSR value to minimize the mean absolute error (MAE) as the true object scene is known. The Wiener filter utilized the point spread function (PSF) of the imaging system outlined in Table 1, along with the estimated atmospheric coherence diameter determined from the reduction in warping during image restoration as discussed in the previous paper.

The second algorithm used in this evaluation is the Sobolev gradient flow (SOB) plus Laplacian (LAP) referred to in the literature as SOB+LAP[14]. This algorithm mitigates turbulence in two parts by using a Laplacian operator to mitigate temporal distortions in the imagery. The second part involves using a Sobolev gradient method to sharpen the content in the individual frames. The MATLAB code for the SOB+LAP algorithm is available online[15]. The SOB+LAP & Lucky Look algorithm does require a degraded video sequence and outputs a restored sequence. This capability is very useful for applications when a restored video sequence is required over the whole input sequence. The output video sequence can be temporally averaged to produce a single frame result. The SOB+LAP output data sequence could also be further processed with a Lucky Look fusion[6] approach as done in this paper. The Lucky Look fusion Gaussian blur parameter was optimized to yield the best MAE.

The third algorithm used to process the noisy turbulent data is the bispectral speckle imaging method[7,8,16]. Once again as in a previous paper[5] the apodization used 16×16 pixel tiles[8]. These tiles were also locally registered to provide better performance. The NSR was once again optimized to produce the smallest MAE. The algorithms processed a 25, 50, 75, and 100 frame sequence over 4 levels of turbulence strength.

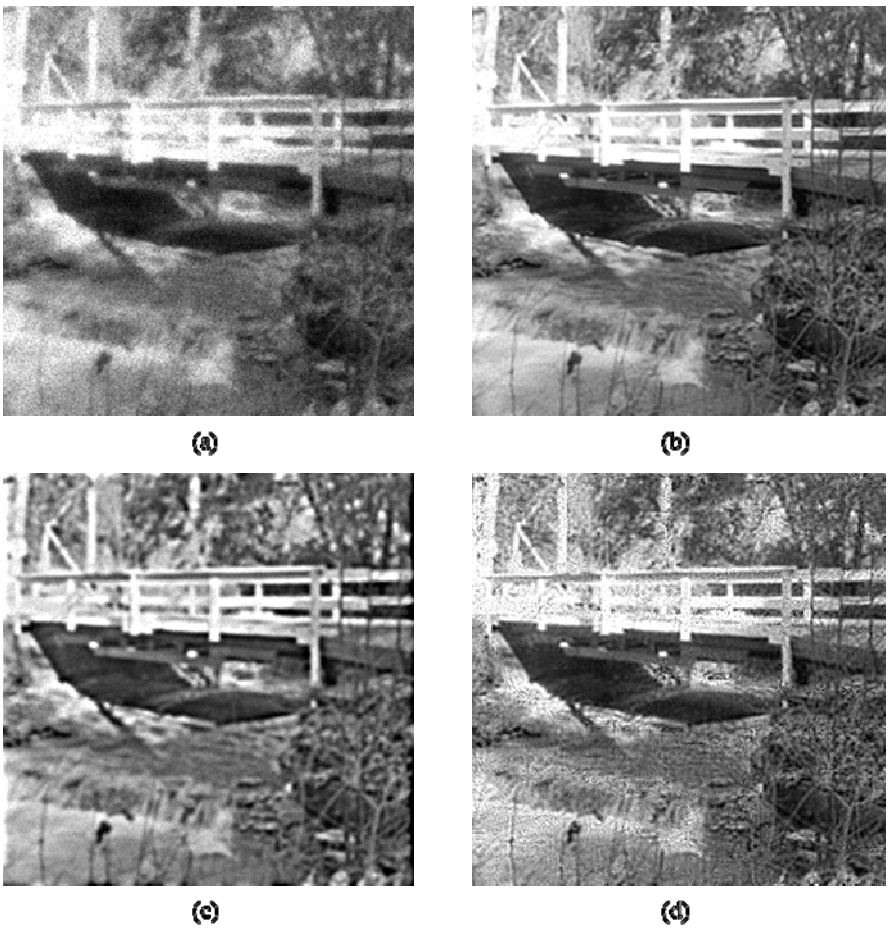

Figure 1. Comparison of processed noisy turbulent data over a 100 frame sequence where the $C_n^2 = 1.0 \times 10^{-16}$ $m^{-2/3}$. (a) an observed noisy turbulent frame, (b) the BMWF turbulence mitigation system, (c) the SOB+LAP with Lucky Look fusion, and (d) the bispectral speckle imaging method.

In the imagery above it is clear to see in Fig. 1(a) the impact from both turbulence and noise. The subsequent imagery in Fig.1 shows the final output frame after processing 100 frames of noisy turbulent data with a constant $C_n^2 = 1.0\times10^{-16}$ $m^{-2/3}$. The BMWF algorithm balances the noise suppression along with deblurring the imagery. In the SOB+LAP & Lucky Look case the noise is significantly reduced. The image though appears to have less of the higher frequency content present in Fig. 1(b). In the bispectral speckle imaging case the imagery retains higher spatial frequencies. There is a small residual amount of noise in the imagery.

Fig.1 showcases one specific data point with varying levels of turbulence with and without noise. A more comprehensive overview of the results is shown in Fig.2. As the number of frames increase it is expected in the generic case of simple temporal averaging that the SNR will increase. As algorithms try to make smarter decisions about what patches contain higher frequency content they could potentially not use all the available frames. In turn, the MAE between the restored result and truth image will be higher than an algorithm that utilizes the information in all the frames. This is case between the BMWF and the SOB+LAP & Lucky Look. The SOB+LAP & Lucky Look holds the same MAE as the number of frames increase for just one turbulence case. The difference between the clean and noisy case becomes harder to distinguish for the SOB+LAP & Lucky Look algorithm as the turbulence increases.

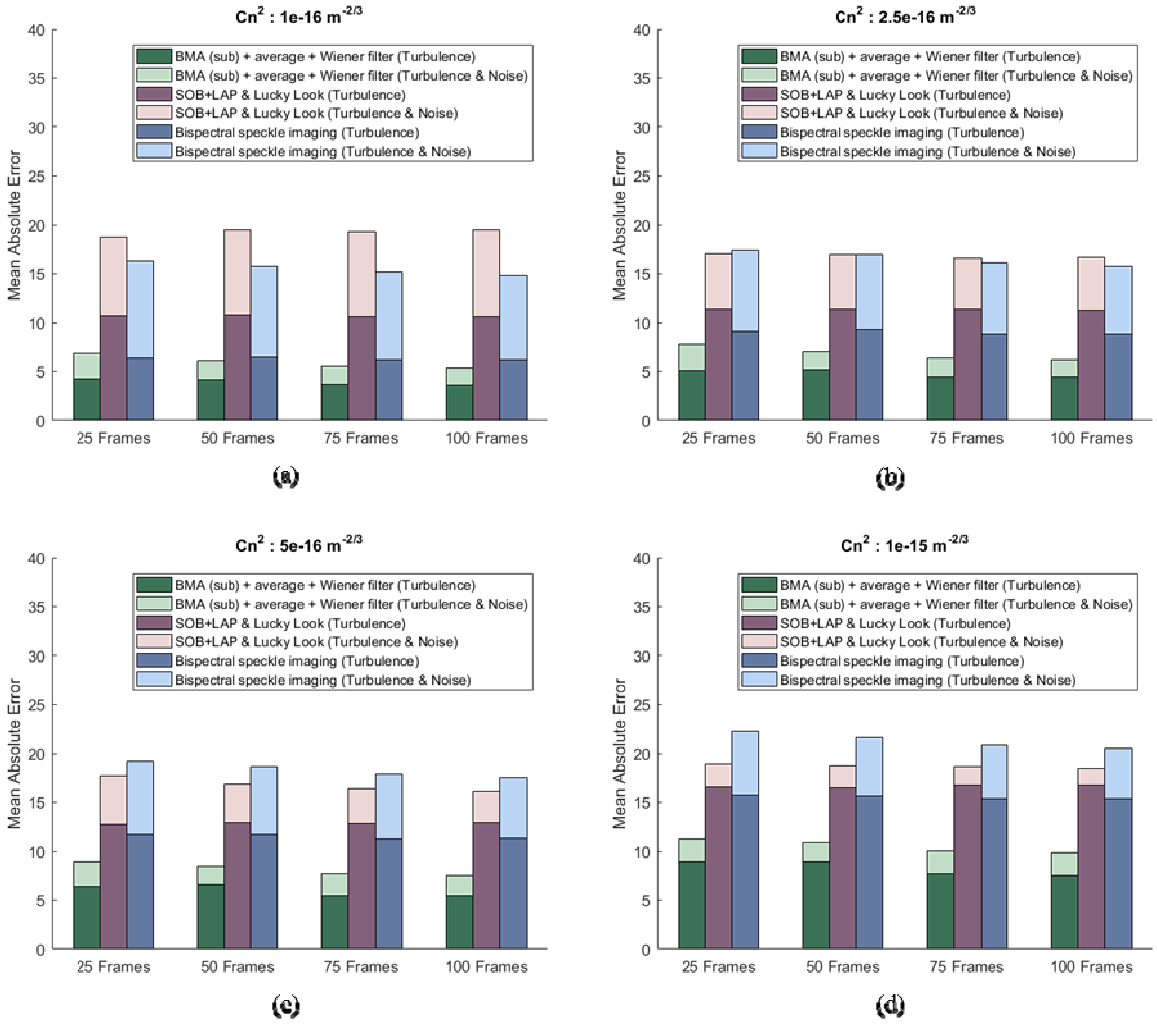

Figure 2. Overview of the algorithms performance with varying levels of input frames and turbulence levels.

The BMWF algorithm shows consistent performance. The turbulence only case has a slowly decreasing MAE as there are more frames. Noise in the imagery only causes a slight increase in the MAE. Finally, the bispectral speckle imaging also holds a steady MAE with and without noise over varying levels of turbulence. It is important to remember some portions of the algorithms used tuned NSR values to produce the best MAE value. In real applications the true scene is not available to help optimize the algorithm.

4. CONCLUSION

In this paper we have examined how well noisy anisoplanatic turbulent data is restored by the BMWF turbulence mitigation system, SOB+LAP & Lucky Look, and a bispectral speckle algorithm. The Poisson-Gaussian noise model helped to add appropriate noise to the short exposure turbulence simulated data sets. A short integration time required to freeze the turbulence results in lower SNR imagery. The joint turbulence and low SNR datasets provide an accurate imaging scenario. Each algorithm provides different MAE trends throughout the various number of frames and turbulence strength datasets. The survey indicates that utilizing all the information in the time domain for short exposure imagery yields the best results.

ACKNOWLEDGMENTS

The work used in this paper has been supported in part by funding from L-3 Communications Cincinnati Electronics and under AFRL Award Nos. FA8650-10-2-7028 and FA9550-14-1-0244.

REFERENCES

[1] Michael C Roggemann, Byron M. Welsh, and Bobby R. Hunt. [Imaging through turbulence]. CRC press, (1996).
[2] David L. Fried, "Limiting resolution looking down through the atmosphere." JOSA 56.10, 1380-1384 (1966)
[3] Svetlana L. Lachinova, et al. "Anisoplanatic imaging through atmospheric turbulence: Brightness function approach." Optical Engineering+ Applications. International Society for Optics and Photonics, (2007)
[4] Russell C Hardie, et al. "Simulation of anisoplanatic imaging through optical turbulence using numerical wave propagation with new validation analysis." Optical Engineering 56.7, 071502-071502 (2017)
[5] Russell C Hardie, et al "Block matching and Wiener filtering approach to optical turbulence mitigation and its application to simulated and real imagery with quantitative error analysis." Optical Engineering 56.7, 071503-071503 (2017)
[6] Mathieu Aubailly, et al. "Automated video enhancement from a stream of atmospherically-distorted images: the lucky-region fusion approach." SPIE Optical Engineering+ Applications. International Society for Optics and Photonics, (2009)
[7] Taylor W Lawrence, et al. "Extended-image reconstruction through horizontal path turbulence using bispectral speckle interferometry." Optical Engineering 31.3, 627-636 (1992)
[8] Carmen J Carrano, "Speckle imaging over horizontal paths." International Symposium on Optical Science and Technology. International Society for Optics and Photonics, (2002)
[9] Dalong Li, Russell M. Mersereau, and Steven Simske. "Atmospheric turbulence-degraded image restoration using principal components analysis." IEEE Geoscience and Remote Sensing Letters 4.3, 340-344 (2007)
[10] Luxin Yan, et al. "Atmospheric-turbulence-degraded astronomical image restoration by minimizing second-order central moment." IEEE Geoscience and Remote Sensing Letters 9.4, 672-676 (2012)
[11] Michael Rucci, Russell C. Hardie, and Kenneth J. Barnard. "Computationally efficient video restoration for Nyquist sampled imaging sensors combining an affine-motion-based temporal Kalman filter and adaptive Wiener filter." Applied optics 53.13, C1-C13. (2014)
[12] Markku Mäkitalo, and Alessandro Foi. "Poisson-gaussian denoising using the exact unbiased inverse of the generalized anscombe transformation." Acoustics, Speech and Signal Processing (ICASSP), 2012 IEEE International Conference on. IEEE, (2012)
[13] Donald Fraser, Glen Thorpe, and Andrew Lambert. "Atmospheric turbulence visualization with wide-area motion-blur restoration." JOSA A 16.7, 1751-1758 (1999)
[14] Y Lou, S H Kang, S Soatto, and A L Bertozzi. Video stabilization of atmospheric turbulence distortion. Inverse Problems in Imaging, Special Issue in honor of Tony Chan,7(3), 839 - 861 (2013)
[15] https://sites.google.com/site/louyifei/research/turbulence
[16] Glen E Archer, Jeremy P. Bos, and Michael C. Roggemann. "Comparison of bispectrum, multiframe blind deconvolution and hybrid bispectrum-multiframe blind deconvolution image reconstruction techniques for anisoplanatic, long horizontal-path imaging." Optical Engineering 53.4, 043109-043109 (2014)